Mechanism of GlvA from *Bacillus subtilis*: A Detailed Kinetic Analysis of a 6-Phospho-α-glucosidase from Glycoside Hydrolase Family 4[†]

Vivian L. Y. Yip,[‡] John Thompson,[§] and Stephen G. Withers*[,‡]

Department of Chemistry, University of British Columbia, 2036 Main Mall, Vancouver, BC, Canada V6T 1Z1, and Microbial Biochemistry and Genetics Unit, Oral Infection and Immunity Branch, NIDCR, Bethesda, Maryland 20892

Received March 16, 2007; Revised Manuscript Received June 7, 2007

ABSTRACT: GlvA, a 6-phospho-α-glucosidase from *Bacillus subtilis* assigned to glycoside hydrolase family 4, catalyzes the hydrolysis of maltose 6′-phosphate via a redox-elimination−addition mechanism requiring NAD^+ as cofactor. In contrast to previous reports and consistent with the proposed mechanism, GlvA is only activated in the presence of the nicotinamide cofactor in its oxidized, and not the reduced NADH, form. Significantly, GlvA catalyzes the hydrolysis of *both* 6-phospho-α- and 6-phospho-*β*-glucosides containing activated leaving groups such as *p*-nitrophenol and does so with retention and inversion, respectively, of anomeric configuration. Mechanistic details of the individual bond cleaving and forming steps were probed using a series of 6-phospho-α- and 6-phospho-*β*-glucosides. Primary deuterium kinetic isotope effects (KIEs) were measured for both classes of substrates in which either the C2 or the C3 protons have been substituted with a deuterium, consistent with C−H bond cleavage at each center being partially rate-limiting. Kinetic parameters were also determined for 1-[^{2}H]-substituted substrates, and depending on the substrates and the reaction conditions, the measurements of k_{cat} and k_{cat}/K_M produced either no KIEs or inverse KIEs. In conjunction with results of Brønsted analyses with both aryl 6-phospho-α- and *β*-glucosides, the kinetic data suggest that GlvA utilizes an $E1_{cb}$ mechanism analogous to that proposed for the *Thermotoga maritima* BglT, a 6-phospho-*β*-glucosidase in glycoside hydrolase family 4 (Yip, V.L.Y et al. (2006) *Biochemistry 45*, 571−580). The pattern of isotope effects measured and the observation of very similar k_{cat} values for all substrates, including unactivated and natural substrates, indicate that the oxidation and deprotonation steps are rate-limiting steps in essentially all cases. This mechanism permits the cleavage of both α- and *β*-glycosides within the same active site motif and, for activated substrates that do not require acid catalysis for cleavage, within the same active site, yielding the product sugar-6-phosphate in the same anomeric form in the two cases.

Glycoside hydrolases comprise a large class of enzymes that catalyze the hydrolysis of glycosidic linkages. An abundance of structural and mechanistic data is available for these enzymes, and this information is catalogued in the frequently updated CAZY website (http://www.cazy.org/index.html) (*1*, *2*), which groups glycosidases into different families on the basis of primary sequence similarity. Clans have also been established to assemble different families that share similar structures (*3*). Enzymes belonging to the same glycoside hydrolase family have structural and mechanistic commonalities (*2*, *3*), with the vast majority using either a direct or a double displacement mechanism with inversion or retention of the substrate anomeric configuration, respectively (*4*−*6*). Of the more than 100 different families described thus far, only glycoside hydrolase family 4 (GH4[1]) contains both α- and *β*-glycosidases. All other glycoside hydrolase families contain only enzymes that display the same specificity for substrate anomeric configuration[2]. GH4

[†] This work was supported by grants from the Natural Sciences and Engineering Research Council of Canada, the Protein Engineering Network of Centres of Excellence of Canada, the Canadian Institutes of Health Research, and by the NIDCR Intramural Research Program of the National Institutes of Health. V.L.Y.Y. is funded by the Michael Smith Foundation for Health Research.

* To whom correspondence should be addressed. Tel: (604) 822-3402. Fax: (604) 822-8869. E-mail: withers@chem.ubc.ca.

[‡] University of British Columbia.

[§] NIDCR.

[1] Abbreviations: 4C2NP*β*G6P, 4-chloro-2-nitrophenyl 6-phospho-*β*-D-glucoside; 4CNP*β*G6P, 4-cyanophenyl 6-phospho-*β*-D-glucoside; C6′P, cellobiose 6′-phosphate; 35DCP*β*G6P, 3,5-dichlorophenyl 6-phospho-*β*-D-glucoside; 24DNP*β*G6P, 2,4-dinitrophenyl 6-phospho-*β*-D-glucoside; 25DNP*β*G6P, 2,5-dinitrophenyl 6-phospho-*β*-D-glucoside; 34DNPαG6P, 3,4-dinitrophenyl 6-phospho-α-D-glucoside; 34DNP*β*G6P, 3,4-dinitrophenyl 6-phospho-*β*-D-glucoside; ESI MS, electrospray ionization mass spectrometry; G6P, glucose 6-phosphate; G6PDH, glucose 6-phosphate dehydrogenase; GH4, glycoside hydrolase family 4; KIE, kinetic isotope effect; M6′P, maltose 6′-phosphate; MeαG6P, methyl 6-phospho-α-D-glucoside; 1[^{2}H]MeαG6P, methyl 1-[^{2}H]-6-phospho-α-D-glucoside; Me*β*G6P, methyl 6-phospho-*β*-D-glucoside; NAD^+, *β*-nicotinamide adenine dinucleotide; NADH, *β*-nicotinamide adenine dinucleotide, reduced; $NADP^+$, *β*-nicotinamide adenine dinucleotide phosphate; NADPH, *β*-nicotinamide adenine dinucleotide phosphate, reduced; 2NP*β*G6P, 2-nitrophenyl 6-phospho-*β*-D-glucoside; 3NP*β*G6P, 3-nitrophenyl 6-phospho-*β*-D-glucoside; 4NPαG6P, 4-nitrophenyl 6-phospho-α-D-glucoside; 1[^{2}H]4NPαG6P, 4-nitrophenyl 1-[^{2}H]-6-phospho-α-D-glucoside; 2[^{2}H]4NPαG6P, 4-nitrophenyl 2-[^{2}H]-6-phospho-α-D-glucoside; 3[^{2}H]4NPαG6P, 4-nitrophenyl 3-[^{2}H]-6-phospho-α-D-glucoside; 4NP*β*G6P, 4-nitrophenyl 6-phospho-*β*-D-glucoside; 1[^{2}H]4NP*β*G6P, 4-nitrophenyl 1-[^{2}H]-6-phospho-*β*-D-glucoside; 2[^{2}H]4NP*β*G6P, 4-nitrophenyl 2-[^{2}H]-6-phospho-*β*-D-glucoside; 3[^{2}H]4NP*β*G6P, 4-nitrophenyl 3-[^{2}H]-6-phospho-*β*-D-glucoside; PαG6P, phenyl 6-phospho-α-D-glucoside; P*β*G6P, phenyl 6-phospho-*β*-D-glucoside; UV−vis, ultraviolet−visible.

10.1021/bi700536p CCC: $37.00
Published on Web 08/04/2007

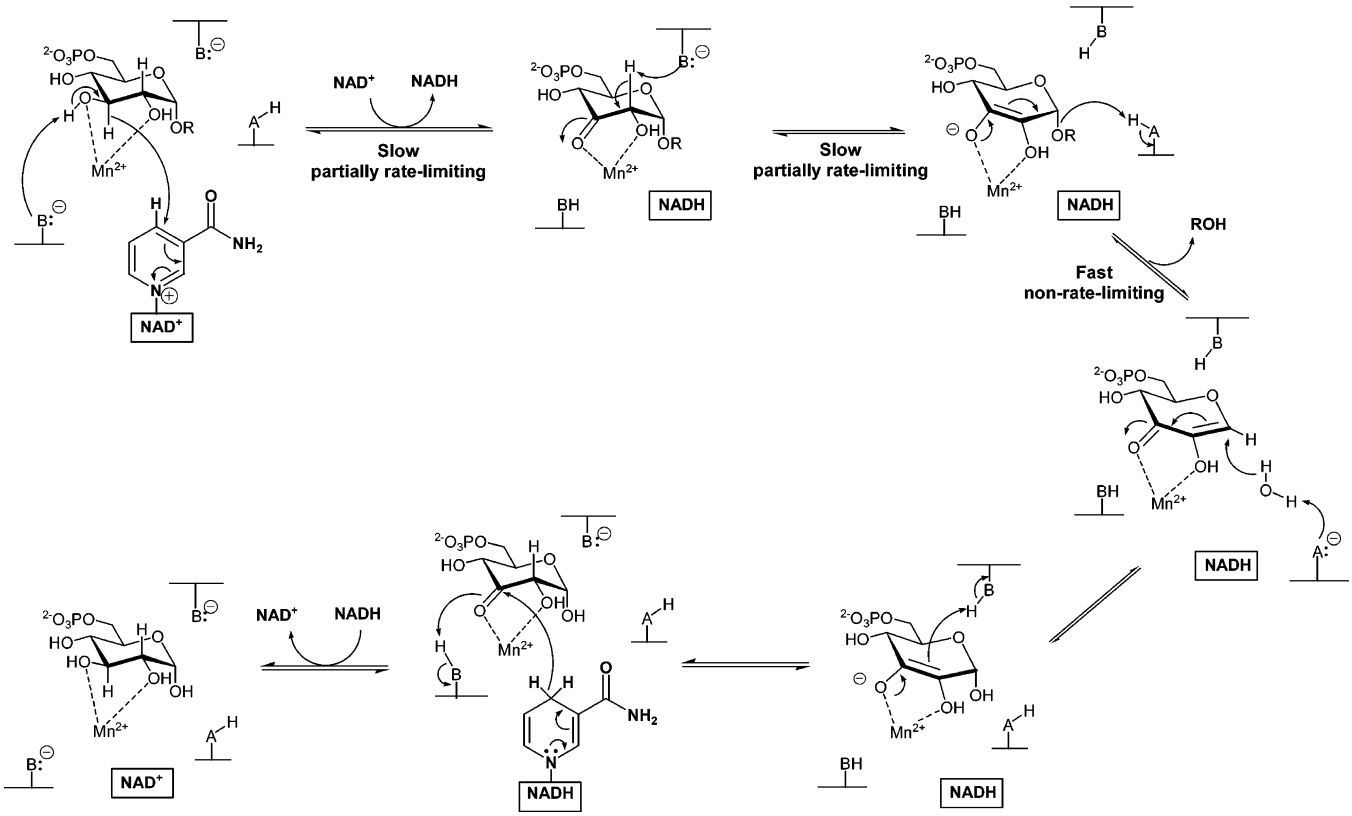

FIGURE 1: Proposed $E1_{cb}$ mechanism of GlvA.

enzymes are uniquely identifiable by their absolute requirement for both NAD^+, a divalent metal (Mn^{2+}, Ni^{2+}, Co^{2+}, Mg^{2+}, or Ca^{2+}), and reducing conditions for catalytic activity (*7*−*13*). GH4 enzymes have been found to employ an elimination mechanism rather than the traditional nucleophilic displacement mechanisms (*13*−*16*).

The unusual properties of GH4 enzymes have recently been studied through a number of structural and mechanistic analyses. A common mechanism has been proposed for both the α- and *β*-glycosidases in this family. Key steps in the proposed reaction include (1) C3 hydride abstraction by the NAD^+ cofactor and consequent oxidation of the C3 hydroxyl; (2) abstraction of the C2 proton via general base catalysis; (3) α,*β*-elimination of the aglycone; (4) 1,4-Michael-like addition of water to the α,*β*-unsaturated intermediate; (5) reprotonation at C2; and finally (6) reduction of the C3 carbonyl via oxidation of the on-board NADH cofactor (Figure 1) (*13*, *15*, *16*).

Detailed mechanistic analysis has been reported for a GH4 6-phospho-*β*-glucosidase, BglT from *Thermotoga maritima* (*14*), with the proposed mechanism being originally derived from a key piece of evidence. Solvent deuterium exchange at the C2 position was observed when the enzymatic reaction was carried out in D_2O, indicating that the C2−H2 bond is cleaved (*13*). Subsequent X-ray crystallographic data, kinetic isotope effect measurements, and Brønsted analyses provided strong support for this hypothesis (*14*, *15*). The NAD^+ cofactor found in the active site of the enzyme was perfectly oriented with respect to the substrate for abstraction of the C3 hydride. Primary kinetic isotope effects indicated that oxidation of the C3 hydroxyl and deprotonation of C2 are both partially rate-limiting. In contrast, cleavage of the C1−O1 bond is relatively fast, as indicated by the flat Brønsted plots and absence of an isotope effect at C1, which is suggestive of an $E1_{cb}$-type mechanism (*14*).

The 6-phospho-α-glucosidase, GlvA, was proposed to undergo the same redox-elimination−addition mechanism on the basis of the observation of solvent deuterium incorporation into the substrate and X-ray crystallographic data (*16*). However, despite these results, the details of the reaction steps have not yet been established for any GH4 α-glycosidases. This is of importance because GlvA catalyzes the hydrolysis of *both* 6-phospho-α- and 6-phospho-*β*-glycosides containing activated leaving groups such as *p*-nitrophenol. Accordingly, a detailed mechanistic analysis of GlvA was required to provide a solid mechanistic understanding of both α- and *β*-glycosidic bond cleavage by GH4 enzymes. Such an analysis is provided in this article.

MATERIALS AND METHODS

General Methods. All NMR spectra were recorded on Bruker Avance 300 and Bruker Avance 400 spectrometers at 300 and 400 MHz, respectively. All NMR spectra were collected at neutral pH. Chemical shifts are reported on the *δ* scale in parts per million from tetramethylsilane (TMS) and were referenced to D_2O. ^{31}P NMR signals were externally referenced to 85% H_3PO_4 in H_2O, and ^{19}F NMR signals were externally referenced to CF_3COOH. Low- and high-resolution mass spectra were collected by the mass spectrometry laboratory at the University of British Colum-

[2] The presence of both α-L-iduronidases and *β*-D-xylosidases (Nieman et al. (2003) *Biochemistry 42*, 8054−8065) in GH39 does not indicate any inherent problem with family classifications because the absolute anomeric configurations of α-L-iduronides and *β*-D-xylosides are the same. The apparent discrepancy is a consequence of the nomenclature rules for D- and L-sugars.

bia. Elemental analysis was performed by Minaz Lakha of the microanalysis laboratory at the University of British Columbia. Preparation of GlvA was as described by Thompson et al. (*10*).

Materials. All chemicals and reagents were purchased from Sigma-Aldrich unless stated otherwise. All solvents were freshly distilled except where mentioned. Column chromatography was performed on 230−400 mesh silica gel.

Synthesis of Aryl Glucosides. The syntheses of all aryl 6-phospho-β-D-glucosides as well as cellobiose 6′-phosphate were reported in Yip et al. (*14*). *p*-Nitrophenyl α-D-glucopyranoside was purchased from Sigma-Aldrich. 3-[^{2}H]-D-Glucopyranose was synthesized on the basis of published procedures (*17*, *18*) from 1,2:5,6-di-*O*-isopropylidene-α-D-ribo-3-hexulofuranulose hydrate, which was purchased from CMS Chemicals Ltd. 1-[^{2}H]-D-Glucopyranose and 2-[^{2}H]-D-glucopyranose were purchased from Cambridge Isotope Laboratories, Inc. The deuterated *p*-nitrophenyl 2,3,4,6-tetra-*O*-acetyl-α-D-glucopyranosides were synthesized from deuterated 1,2,3,4,6-penta-*O*-acetyl-D-glucopyranose using stannic chloride catalyst as described by Audichya et al. (*19*) with minor modifications. All other aryl α-D-glucosides were synthesized from 1,2,3,4,6-penta-*O*-acetyl-D-glucopyranose. Phenyl 2,3,4,6-tetra-*O*-acetyl-α-D-glucopyranoside was synthesized by the stannic chloride-catalyzed glycosidation of phenol. 3,4-Dinitrophenyl 2,3,4,6-tetra-*O*-acetyl-α-D-glucopyranoside was synthesized using the BF_3-diethyl etherate catalyzed method described by Lee et al. (*20*). 3,4-Dinitrophenyl 2,3,4,6-tetra-*O*-acetyl-α-D-glucopyranoside was deprotected with HCl in methanol (*21*). All other aryl α-D-glucosides were deprotected using sodium methoxide in methanol (*22*). Selective phosphorylation at O6 of aryl α-D-glucosides was accomplished with $POCl_3$ according to published procedures (*23*) with minor modifications. Methyl α-D-glucoside and methyl β-D-glucoside were phosphorylated using diphenyl chlorophosphate and deprotected via catalytic hydrogenation essentially as described by Cawley et al. (*24*). The synthesis of maltose 6′-phosphate will be published elsewhere. Characterization of the products is provided below.

4-Nitrophenyl 6-Phospho-α-D-glucoside (4NPαG6P). ^{1}H NMR (400 MHz, D_2O) δ 8.10 (2 H, d, $J_{Ar2,Ar3} = J_{Ar5,Ar6} =$ 9.2 Hz, Ar3, Ar5), 7.15 (2 H, d, $J_{Ar2,Ar3} = J_{Ar5,Ar6} = 9.2$ Hz, Ar2, Ar6), 5.66 (1 H, d, $J_{1,2} = 3.6$ Hz, H1), 3.92−3.87 (1 H, m, $H6_a$), 3.83−3.78 (1 H, m, H3), 3.69−3.57 (4 H, m, H2, H4, H5, $H6_b$); ^{13}C NMR (100 MHz, D_2O) δ 161.35 (C), 142.24 (C), 125.96 (2 CH), 116.65 (2 CH), 96.72 (C1), 72.51 (d, $J_{5,P} = 7.2$ Hz, C5), 72.21, 70.99, 68.17, 61.92 (d, $J_{6,P} =$ 4.0 Hz, C6); ^{31}P NMR (162 MHz, D_2O) δ 4.80 (t, $J_{H6,P} =$ 5.8 Hz); ESI-MS *m*/*z*: calcd for $[C_{12}H_{15}NO_{11}PNa_2]^+$ 426.0178. Found: 426.0180. Anal. Calcd for $C_{12}H_{14}NNa_2O_{11}P{\cdot}3H_2O$: C, 30.07; H, 4.21; N, 2.92. Found: C, 30.47; H, 3.93; N, 2.70.

4-Nitrophenyl 1-[^{2}H]-6-Phospho-α-D-glucoside (1[^{2}H]-4NPαG6P). ^{1}H NMR (400 MHz, D_2O) δ 8.12 (2 H, d, $J_{Ar2,Ar3} = J_{Ar5,Ar6} = 9.3$ Hz, Ar3, Ar5), 7.15 (2 H, d, $J_{Ar2,Ar3} = J_{Ar5,Ar6} = 9.3$ Hz, Ar2, Ar6), 3.92−3.86 (1 H, m, $H6_a$), 3.81 (1 H, t, $J_{2,3} = J_{3,4} = 9.3$ Hz, H3), 3.69−3.57 (4 H, m, H2, H4, H5, $H6_b$); ^{13}C NMR (100 MHz, D_2O) δ 161.35 (C), 142.24 (C), 125.95 (2 CH), 116.66 (2 CH), 72.50 (d, $J_{5,P} = 6.7$ Hz, C5), 72.21, 70.90, 268.19, 61.91 (d, $J_{6,P} = 5.8$ Hz, C6); ^{31}P NMR (121 MHz, D_2O) δ 5.54 (t, $J_{H6,P} = 6.1$ Hz); ESI-MS *m*/*z*: calcd for $[C_{12}H_{14}DNO_{11}PNa_2]^+$ 427.0241. Found: 427.0239.

4-Nitrophenyl 2-[^{2}H]-6-Phospho-α-D-glucoside (2[^{2}H]-4NPαG6P). ^{1}H NMR (400 MHz, D_2O) δ 8.13 (2 H, d, $J_{Ar2,Ar3} = J_{Ar5,Ar6} = 9.3$ Hz, Ar3, Ar5), 7.17 (2 H, d, $J_{Ar2,Ar3} = J_{Ar5,Ar6} = 9.3$ Hz, Ar2, Ar6), 5.67 (1 H, s, H1), 3.90 (1 h, ddd, $J =$ 12.4, 7.7, 2.6 Hz, $H6_a$), 3.81 (1 H, d, $J_{3,4} = 8.8$ Hz, H3), 3.66−3.58 (3 H, m, H4, H5, $H6_b$); ^{13}C NMR (100 MHz, D_2O) δ 161.34 (C), 142.23 (C), 125.95 (2 CH), 116.64 (2 CH), 96.69 (C1), 72.54 (d, $J_{5,P} = 6.9$ Hz, C5), 72.13, 68.16, 61.84 (d, $J_{6,P} = 4.6$ Hz, C6); ^{31}P NMR (162 MHz, D_2O) δ 4.98 (t, $J_{H6,P} = 5.2$ Hz); ESI-MS *m*/*z*: calcd for $[C_{12}H_{14}DNO_{11}PNa_2]^+$ 427.0241. Found: 427.0243. Anal. Calcd for $C_{12}H_{13}DNNa_2O_{11}P{\cdot}4H_2O$: C, 28.91; H, 4.62; N, 2.81. Found: C, 29.27; H, 4.96; N, 2.92.

4-Nitrophenyl 3-[^{2}H]-6-Phospho-α-D-glucoside (3[^{2}H]-4NPαG6P). ^{1}H NMR (400 MHz, D_2O) δ 8.13 (2 H, d, $J_{Ar2,Ar3} = J_{Ar5,Ar6} = 9.3$ Hz, Ar3, Ar5), 7.16 (2 H, d, $J_{Ar2,Ar3} = J_{Ar5,Ar6} = 9.3$ Hz, Ar2, Ar6), 5.67 (1 H, d, $J_{1,2} = 3.7$ Hz, H1), 3.90 (1 H, ddd, $J = 12.2$, 7.6, 2.6 Hz, $H6_a$), 3.69−3.58 (4 H, m, H2, H4, H5, $H6_b$); ^{13}C NMR (75 MHz, D_2O) δ 162.85 (C), 143.75 (C), 127.46 (2 CH), 118.17 (2 CH), 98.24 (C1), 74.05 (d, $J_{5,P} = 7.1$ Hz, C5), 72.45, 69.61, 63.41 (d, $J_{6,P} = 5.4$ Hz, C6); ^{31}P NMR (162 MHz, D_2O) δ 4.88 (t, $J_{H6,P} = 6.1$ Hz); ESI-MS *m*/*z*: calcd for $[C_{12}H_{14}DNO_{11}PNa_2]^+$ 427.0241. Found: 427.0239. Anal. Calcd for $C_{12}H_{13}DNNa_2O_{11}P{\cdot}5.5H_2O$: C, 27.43; H, 4.95; N, 2.67. Found: C, 26.96; H, 4.51; N, 2.46.

Maltose 6′-Phosphate (M6′P). ^{1}H NMR (400 MHz, D_2O) δ 5.25 (1 H, d, $J_{1',2'} = 3.7$ Hz, H1′), 5.10 (1 H, d, $J_{\alpha1,\alpha2} =$ 3.6 Hz, αH1), 4.52 (1 H, d, $J_{\beta1,\beta2} = 8.0$ Hz, βH1), 0.27−7.24 (2 H, m, Ar), 7.06−7.00 (3 H, m, Ar), 5.50 (1 H, d, $J_{1,2} = 3.7$ Hz, H1), 3.95−3.87 (1 H, m), 3.80 (1 H, t, $J =$ 9.3 Hz), 3.70−3.56 (4 H, m); ^{13}C NMR (100 MHz, D_2O) δ 99.99, 99.95, 95.91, 92.02, 77.45, 77.38, 76.30, 74.71, 74.09, 73.33, 72.66, 72.24, 72.01, 71.93, 71.39, 70.08, 69.00, 63.03, 60.82, 60.60; ^{31}P NMR (162 MHz, D_2O) δ 4.04; ESI-MS *m*/*z*: calcd for $[C_{12}H_{22}O_{14}PNa_2]^+$ 467.0546. Found: 467.0543.

Phenyl 6-Phospho-α-D-glucoside (PαG6P). ^{1}H NMR (300 MHz, D_2O) δ 7.27−7.24 (2 H, m, Ar), 7.06−7.00 (3 H, m, Ar), 5.50 (1 H, d, $J_{1,2} = 3.7$ Hz, H1), 3.95−3.87 (1 H, m), 3.80 (1 H, t, $J = 9.3$ Hz), 3.70−3.56 (4 H, m); ^{13}C NMR (100 MHz, D_2O) δ 155.83 (C), 129.80 (2 CH), 123.02 (C), 117.05 (2 CH), 97.04 (C1), 72.31, 72.11 (d, $J_{5,P} = 7.0$ Hz, C5), 71.13, 68.34, 61.90 (d, $J_{6,P} = 4.2$ Hz, C6); ^{31}P NMR (162 MHz, D_2O) δ 5.49 (1 P, t, $J_{6H,P} = 6.5$ Hz); ESI-MS *m*/*z*: calcd 381.0327; found, 381.0325.

3,4-Dinitrophenyl 6-Phospho-α-D-glucoside (34DNPαG6P). ^{1}H NMR (400 MHz, D_2O) δ 8.03 (1 H, d, $J_{Ar5,Ar6} = 9.2$ Hz, Ar5), 7.55 (1 H, d, $J_{Ar2,Ar6} = 2.4$ Hz, Ar2), 7.39 (1 H, dd, $J_{Ar5,Ar6} = 2.4$ Hz, Ar6), 5.68 (1 H, d, $J_{1,2} = 3.6$ Hz, H1), 3.91−3.85 (1 H, m), 3.77 (1 H, t, $J = 9.3$ Hz), 3.69−3.53 (4 H, m); ^{13}C NMR (100 MHz, D_2O) δ 160.41 (C), 144.67 (C), 135.39 (C), 128.06 (CH), 119.92 (CH), 113.36 (CH), 97.54 (C1), 72.91 (d, $J_{5,P} = 6.5$ Hz, C5), 72.24, 70.95, 68.17, 62.09 (d, $J_{6,P} = 3.8$ Hz, C6); ^{31}P NMR (162 MHz, D_2O) δ 5.55 (1 P, t, $J_{H6,P} = 6.5$ Hz); ESI-MS *m*/*z*: calcd 471.0029; found, 471.0026.

Methyl 6-Phospho-α-D-glucoside (MeαG6P). ^{1}H NMR (400 MHz, D_2O) δ 4.52 (1 H, d, $J_{1,2} = 3.7$ Hz, H1), 3.81−3.68 (2 H, m, $H6_a$, $H6_b$), 3.44−3.24 (4 H, m, H2, H3, H4, H5), 3.13 (3 H, s, CH_3); ^{13}C NMR (100 MHz, D_2O) δ 99.30

(C1), 72.61, 71.17, 70.84 (1 C, d, $J_{5,P} = 7.4$ Hz, C5), 68.79, 62.83 (1 C, d, $J_{6,P} = 4.4$ Hz, C6), 55.02; ^{31}P NMR (121 MHz, D_2O) δ 3.90 (1 P, t, $J_{6H,P} = 4.6$ Hz); ESI-MS *m*/*z*: calcd 319.0171; found, 319.0170. Anal. Calcd for $C_7H_{13}O_9PNa_2 \cdot 0.5H_2O$: C, 25.69; H, 4.28. Found: C, 25.59; H, 4.58.

Methyl 1-[^{2}H]-6-Phospho-α-D-glucoside (1[^{2}H]MeαG6P). ^{1}H NMR (400 MHz, D_2O) δ 3.92−3.86 (1 H, m, H6$_a$), 3.77−3.73 (1 H, m, H6$_b$), 3.53−3.39 (4 H, m, H2, H3, H4, H5), 3.24 (3 H, s, CH_3); ^{13}C NMR (100 MHz, D_2O) δ 98.85 (t, $J_{1,D} = 24.9$ Hz, C1), 72.37, 71.04−70.94 (2 C), 68.54, 62.13 (d, $J_{6,P} = 3.9$ Hz, C6), 54.85 (CH_3); ^{31}P NMR (162 MHz, D_2O) δ 5.58 (1 P, t, $J_{6H,P} = 6.5$ Hz); ESI-MS *m*/*z*: calcd 320.0234; found, 320.0235. Anal. Calcd for $C_7H_{12}DO_9PNa_2 \cdot 2.5H_2O$: C, 23.08 H, 4.95. Found: C, 22.51; H, 4.50.

Methyl 6-Phospho-β-D-glucoside (MeβG6P). ^{1}H NMR (400 MHz, D_2O) δ 4.22 (1 H, d, $J_{1,2} = 8.0$ Hz, H1), 4.01−3.96 (1 H, m, H6$_a$), 3.93−3.88 (1 H, m, H6$_b$), 3.40−3.30 (6 H, m, H3, H4, H5, CH_3), 3.13−3.08 (1 H, m, H2); ^{13}C NMR (100 MHz, D_2O) δ 103.44, 75.60, 74.75 (d, $J_{5,P} = 8.0$ Hz, C5), 73.17, 69.06, 63.88 (d, $J_{6,P} = 4.9$ Hz, C6), 57.41 (CH_3); ^{31}P NMR (121 MHz, D_2O) δ 1.86; ESI-MS *m*/*z*: calcd 319.0171; found, 319.0173. Anal. Calcd for $C_7H_{13}O_9PNa_2 \cdot 2.25H_2O$: C, 23.44; H, 4.92. Found: C, 23.31; H, 4.71.

Enzyme Kinetics. All kinetic assays were conducted in 1 cm path length matched quartz cuvettes with a Cary 300 UV−vis spectrometer equipped with a circulating water bath or a Cary 4000 UV−vis spectrometer attached to a Cary Temperature Controller. Unless stated otherwise, GlvA was preincubated in the assay buffer at 37 °C for 5 min prior to the addition of substrate to initiate the enzymatic reaction. All data fitting was performed with GraFit 4.0 or Cary WinUV, Kinetics Application, Version 3.00.

The following buffer systems were employed: Buffer A, 50 mM HEPES (pH 7.5), 1 mM $MnCl_2$, 0.1 mM NAD^+, 10 mM 2-mercaptoethanol, and 0.1% (w/v) BSA; Buffer B, 50 mM Tris-HCl (pH 8.4), 1 mM $MnCl_2$, 0.1 mM NAD^+, 10 mM 2-mercaptoethanol, and 0.1% (w/v) BSA.

Conditions for the Measurement of Initial Rates. The concentration of GlvA used for each substrate was chosen such that less than 10% of the total substrate was consumed, thus ensuring that linear time courses were measured. GlvA was preincubated with the assay buffer mixture for 5 min, and the reaction was initiated by the addition of the appropriate substrate. The initial rate of hydrolysis was followed spectrophotometrically upon the addition of the appropriate aryl 6-phospho-D-glucoside at the wavelength of maximal absorbance difference between the released phenol and the respective aryl 6-phospho-D-glucoside. The k_{cat} values were calculated using the molecular weight of the subunit at 50513 Da.

Conditions for the Substrate Depletion Method (*25*). The k_{cat}/K_M analyses were performed by the depletion method using low substrate concentrations and by monitoring the change in absorbance at the wavelength of maximal absorbance difference between the released phenol and the respective aryl 6-phospho-D-glucoside until the reaction was complete (approximately 30 min). The data sets were fit to a first-order equation, and the k_{cat}/K_M values were obtained by dividing the pseudo-first-order rate constant by the enzyme concentration.

pH Dependence. GlvA was incubated at a series of pH values, and periodically, aliquots were removed for assay at pH 7.5. These studies revealed that GlvA was stable in the pH range from 4.0 to 10.0. The pH dependence of k_{cat}/K_M was then determined by measurement of k_{cat}/K_M at a series of pH values using the substrate depletion method. All experiments were carried out at 37 °C in 50 mM NaCl, 1 mM $MnCl_2$, 0.1 mM NAD^+, 10 mM 2-mercaptoethanol, and 0.1% (w/v) BSA containing the appropriate buffer system: 20 mM AcOH/NaOAc (pH 4.0−4.5), 20 mM MES (pH 6.1−6.7), 20 mM HEPES (pH 6.5−8.2), or 20 mM CHES (pH 8.4−9.4). The enzyme (final GlvA concentration of 13.1 or 26.2 μg/mL) was preincubated with the above solutions (final assay volume = 1 mL) at 37 °C for 5 min, and 4NPαG6P (final concentration = 6.7 μM) was added to initiate the enzymatic reaction. The k_{cat}/K_M values were obtained by dividing the pseudo-first-order rate constant by the enzyme concentration. The pH dependence of k_{cat}/K_M was fit to an equation describing a reaction governed by two essential ionizations using the program GraFit.

The pH dependence of k_{cat} was then determined by measuring the initial rate of hydrolysis of saturating concentrations of 4NPαG6P at various pH values. All experiments were carried out at 37 °C in 50 mM NaCl, 1 mM $MnCl_2$, 0.1 mM NAD^+, 10 mM 2-mercaptoethanol, and 0.1% (w/v) BSA containing 20 mM AcOH/NaOAc (pH 4.0−4.5), 20 mM MES (pH 6.1−6.7), 20 mM HEPES (pH 6.5−8.2), or 20 mM CHES (pH 8.4−10.0). The enzyme (final concentration of 4.1 μg/mL) was preincubated with the above solutions (final assay volume = 200 μL) at 37 °C for 5 min, and the reaction was initiated by the addition of 4NPαG6P (final concentration = 1.34 or 2.67 mM). The differences in extinction coefficients ($\Delta\epsilon$) between 4NPαG6P and the *p*-nitrophenolate anion at various pH conditions were determined by the method described by Kempton and Withers (*26*). Two different substrate concentrations were used at each pH value to ensure substrate saturation for the determination of V_{max}. The k_{cat} values were calculated from the observed data. The pH dependence of k_{cat} was fit to an equation describing a reaction governed by two essential ionizations using the program GraFit.

Determination of the K_d Value for Mn^{2+}. One milliliter of GlvA (1 mg/mL) was first dialyzed against 5 × 3 L of 50 mM HEPES (pH 7.5) to remove any bound divalent metals prior to manipulation. Samples of dialyzed GlvA (final concentration of 6.5 μg/mL) and Mn^{2+} (varied from 20 μM to 1 mM) were preincubated in 50 mM HEPES (pH 7.5) or 50 mM Tris-HCl (pH 8.4), 0.1 mM NAD^+, 10 mM 2-mercaptoethanol, and 0.1% (w/v) BSA at 37 °C for 5 min, then 4NPαG6P (final concentration >10 K_M) was added to the reaction mixture to give a final volume of 200 μL and initial rates measured. The reaction rate was plotted against the concentration of Mn^{2+} to generate ligand-binding curves.

Determination of the K_d Value for NAD^+. One milliliter of GlvA(1 mg/mL) was first dialyzed against 5 × 3 L of 50 mM HEPES at pH 7.5 to remove any bound NAD^+ prior to manipulation. Samples of dialyzed GlvA (final concentration of 6.5 μg/mL) and NAD^+ (varied from 5 to 100 μM) were preincubated in 50 mM HEPES (pH 7.5) or 50 mM Tris-HCl (pH 8.4), 1 mM $MnCl_2$, 10 mM 2-mercaptoethanol, and 0.1% (w/v) BSA at 37 °C for 5 min, then 4NPαG6P (final concentration >10 K_M) was added to the reaction mixture to give a final volume of 200 μL and initial rates measured.

The reaction rate was plotted against the concentration of NAD^+ to generate ligand-binding curves.

Michaelis−Menten Kinetics of 4NPαG6P and 4NPβG6P. All experiments were carried out in Buffer A or Buffer B. The activity of GlvA was measured with 4NPβG6P or 4NPαG6P by monitoring the release of the *p*-nitrophenolate anion. The initial linear rate of increase in absorbance at 400 nm is measured upon the addition of the substrate. The differences in extinction coefficients ($\Delta\epsilon$) between the substrate and the *p*-nitrophenol released at pH 7.5 and 8.4 were determined by the method described by Kempton and Withers (*26*). The catalytic parameters were determined by a direct fit of the data to the Michaelis−Menten equation.

Stereochemical Outcome Determination. Methanolysis Reaction. All buffers and chemicals were lyophilized twice from 99.9% D_2O. GlvA was exchanged into deuterated buffer solutions via repeated (three times) dilution and concentration using a centrifugal filter unit (Millipore) with a nominal molecular weight limit (NMWL) of 10 kDa. The enzymatic reaction was performed under the following conditions: 50 mM HEPES at pH 7.5, 1 mM $MnCl_2$, 0.1 mM NAD^+, 0.2 mg/mL GlvA, and 5 M CD_3OD. 4NPβG6P (20 mg) was incubated at 37 °C in 5 mL of the above solution, and the reaction was monitored by TLC (2:1:1 1-butanol/H_2O/acetic acid). Upon completion, the enzyme was removed using a 10 kDa NMWL centrifugal filter unit. One-hundred milligrams of Chelex 100 resin (BioRad) was added to the filtrate and stirred at room temperature for 30 min to remove metal ions. The suspension was then filtered, and the solution was lyophilized, then redissolved in D_2O for ^1H NMR analysis.

Kinetic Isotope Effect Measurements. For k_H/k_D measurements, GlvA (final concentration of 3.3 mg/mL (pH 7.5) or 1.6 μg/mL (pH 8.4)) and substrate (final concentration was approximately equal to 10 K_M) were combined to obtain k_{cat} values from initial rates. Reactions were carried out in 1 mL assay volumes. Measurements for substrates, 4NPβG6P, 1[^{2}H]4NPβG6P, 2[^{2}H]4NPβG6P, 3[^{2}H]4NPβG6P, 4NPαG6P, 1[^{2}H]4NPαG6P, 2[^{2}H]4NPαG6P, and 3[^{2}H]4NPαG6P, were repeated at least 6 times each in Buffer A and in Buffer B. Initial rates for the substrates containing the 4-nitrophenol leaving group were measured by monitoring the reaction spectrophotometrically at 400 nm. For MeαG6P and 1[^{2}H]-MeαG6P, initial rates were measured using the G6PDH and $NADP^+$ coupled assay described later in 1 mL assay volumes containing 6.5 μg/mL GlvA, 20 units of G6PDH, 2 mM $NADP^+$, and 8.0 mM substrate. Each measurement was repeated at least 6 times in Buffer A and in Buffer B, and the initial rates of NADPH formation were monitored spectrophotometrically at 340 nm. In each case, the $(k_{cat})_H/(k_{cat})_D$ value was calculated by dividing the rate for the protio substrate by the rate for the deuterio substrate.

For $(k_{cat}/K_M)_H/(k_{cat}/K_M)_D$ measurements, GlvA (final concentration chosen such that the reaction was complete in less than 1 h) was assayed with 4NPβG6P, 1[^{2}H]4NPβG6P, 2[^{2}H]-4NPβG6P, 3[^{2}H]4NPβG6P, 4NPαG6P, 1[^{2}H]4NPαG6P, 2[^{2}H]4NPαG6P, and 3[^{2}H]4NPαG6P (final concentration was chosen such that it was less than 0.2 K_M). The absorbance at 400 nm was monitored until the substrate was depleted. The data set was fitted to a first-order curve, and the k_{cat}/K_M values were obtained by dividing the pseudo-first-order rate constant obtained by the enzyme concentration in each case, with measurements for the protio and deuterio substrate being performed in alternation. Each measurement was repeated 6 times, and the $(k_{cat}/K_M)_H/(k_{cat}/K_M)_D$ value was calculated by dividing each of the pseudo-first-order rate constants for the protio substrate by that obtained for its deuterio substrate partner. For MeαG6P and 1[^{2}H]MeαG6P, the substrate depletion method was used with the G6PDH coupled assay, and the change in absorbance at 340 nm upon formation of NADPH was monitored.

Kinetic and Spectroscopic Investigation of NAD^+ Reduction. For the kinetic analysis, a sample of dialyzed GlvA (final concentration = 3.3 μg/mL = 65 nM) and NAD^+ (final concentration = 100 μM) was preincubated in Buffer A for 5 min, then 4NPαG6P (final concentration of 669 μM > 10 K_M) was added to the reaction mixture (final volume = 200 μL). In a second reaction, dialyzed GlvA (final concentration = 3.3 μg/mL = 65 nM), NAD^+ (final concentration = 100 μM), and $NaBH_4$ (final concentration = 10 mM) were preincubated in Buffer A for 5 min, and 4NPαG6P (final concentration of 669 μM) was added to a final assay volume of 200 μL. The change in A_{400} was monitored for 18 min prior to the addition of 10 μL of 200 μM NAD^+ to rescue enzyme activity. The change in A_{400} was then measured for another 20 min. A similar experiment was repeated in Buffer B.

The absorbance spectra (from 250 to 400 nm) of the following three dialyzed enzyme samples were measured in 1 mL, 1 cm path length-matched quartz cuvettes: 100 μM GlvA; 100 μM GlvA incubated with 100 μM NAD^+; and 100 μM GlvA incubated with 100 μM NAD^+ and 10 mM sodium borohydride. Measurement of sample pH after reaction confirmed that 10 mM sodium borohydride did not significantly alter the pH of the solution.

Glucose 6-Phosphate Dehydrogenase Coupled Assay. MeαG6P and M6′P. Reaction rates for non-chromogenic substrates were measured using a glucose 6-phosphate dehydrogenase (G6PDH and $NADP^+$) coupled assay. All experiments were carried out at 37 °C in Buffer A or Buffer B, containing 2 mM $NADP^+$ and 20 units of G6PDH. and activity was measured spectrophotometrically at 340 nm. Initial rates were measured upon the addition of MeαG6P to the reaction mixture (final volume = 200 μL). Eight to 12 data points were collected under the following conditions: MeαG6P, final substrate concentration range = 100−1700 μM; final enzyme concentration = 6.5 μg/mL (pH 7.5) or 3.3 μg/mL (pH 8.4). Similar conditions were used for M6′P. Seven data points were collected with the following concentration ranges: M6′P, final substrate concentration range = 75−1500 μM; final enzyme concentration = 2.0 μg/mL. The molar extinction coefficient of 6,220 M^{-1} cm^{-1} ($\Delta\epsilon$ of NADPH) was used for the calculation of initial rates of substrate hydrolysis, and the catalytic parameters were determined on the basis of a direct fit of the data to the Michaelis−Menten equation. The concentration of GlvA was doubled for two data points, and the observed rate was also seen to double, confirming that the GlvA reaction was indeed the rate-limiting process. In order to ensure that the presence of $NADP^+$ and G6PDH did not affect the 6-phospho-α-glucosidase activity, GlvA was assayed with 4NPαG6P in the presence of 2 mM $NADP^+$ and, separately, 20 units of G6PDH. In each case, the observed rate was the same as that when GlvA was assayed alone. In addition, an ap-

proximate K_i value for MeαG6P was determined by measuring the reduction in GlvA activity with 4NPαG6P in the presence of MeαG6P. GlvA was added to assay mixtures containing a fixed concentration of 4NPαG6P and varying amounts of MeαG6P. Because MeαG6P and its hydrolyzed products are not chromogenic, inclusion of MeαG6P does not interfere with the detection of the *p*-nitrophenolate anion liberated by the hydrolysis of 4NPαG6P, and MeαG6P can be considered as a competitive inhibitor. (See Determination of K_i.)

Brønsted Analyses. Initial rates were measured for each aryl 6-phospho-β-D-glucoside and aryl 6-phospho-α-D-glucoside in Buffer A and Buffer B using 7−10 different substrate concentrations ranging from 0.7 to 7 K_M. The concentration of GlvA used in the final assay volume of 200 μL was varied from 1.0 to 16 μg/mL. The differences in extinction coefficients ($\Delta\epsilon$) between the aryl 6-phospho-β-D-glucoside and the phenol released at pH 7.5 and at pH 8.4 were determined by the method described by Kempton and Withers (*26*), and these $\Delta\epsilon$ values were used in the calculation of the initial rates of substrate hydrolysis. The catalytic parameters (k_{cat} and K_M) were determined on the basis of a direct fit of the data to the Michaelis−Menten equation.

Determination of K_i. Inhibition studies were performed in Buffer A or Buffer B using the appropriate amount of GlvA (final assay volume = 200 μL). Approximate K_i values were determined by measuring the reduction in rates of GlvA-catalyzed hydrolysis of a fixed concentration of 4NPαG6P, in the presence of varying concentrations of inhibitor. The experiments were repeated at different concentrations of 4NPαG6P. The data were graphed on a Dixon plot ($1/\nu$ vs [competitive inhibitor]). A horizontal line drawn through $1/V_{max}$ in the Dixon plot intersects the experimental lines at an inhibitor concentration equal to $-K_i$.

RESULTS

pH Dependence. The pH dependences of k_{cat} and k_{cat}/K_M were investigated. The plot of k_{cat}/K_M versus pH and the plot of k_{cat} versus pH are shown in Figure 2a and b, respectively. The data were fit to classic bell-shaped curves indicative of two essential ionizable groups, and the pH_{opt} and pK_a values calculated from the fits are summarized in Table 1.

Stereochemical Outcome Determination. Methanolysis Reaction. GlvA was previously shown to be a retaining α-glycosidase (*16*), catalyzing the methanolysis of 4NPαG6P with net retention of the anomeric configuration to yield MeαG6P. Because we had shown that GlvA also hydrolyzes activated aryl 6-phospho-β-glucosides, it was of considerable interest to determine the stereochemical outcome of that reaction too. Therefore, ^1H NMR analysis of the methanolysis of 4NPβG6P was performed, revealing only MeαG6P and the hydrolysis product G6P in the reaction mixture, indicating that the addition of water or methanol to the proposed α,β-unsaturated intermediate occurs at C1 from the axial position regardless of the anomeric configuration of the substrate. Thus, for these substrates, GlvA acts as an inverting glycosidase.

Determination of the K_d Value for Mn^{2+}. GlvA was assayed in the presence of various concentrations of Mn^{2+}, the enzyme being completely inactive in the absence of Mn^{2+}. The data were fit to a simple hyperbolic binding equation and K_d values of 54 μM (pH 7.5) and 99 μM (pH 8.4) for the binding of Mn^{2+} to GlvA determined. The data are summarized in Table 2.

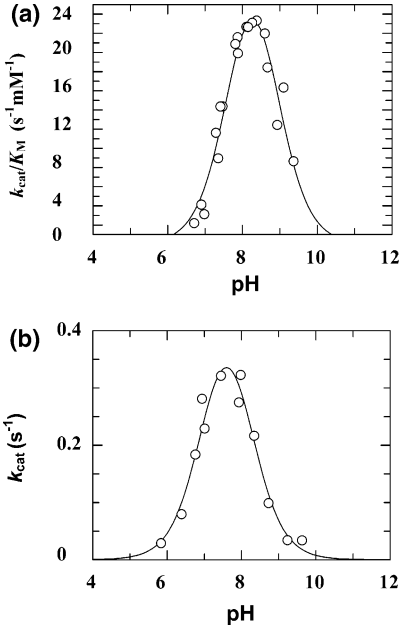

FIGURE 2: pH activity profiles (a) k_{cat}/K_M vs pH and (b) k_{cat} vs pH for the hydrolysis of 4NPαG6P by GlvA.

Table 1: Summary of pK_a Values Determined from the pH Dependence of k_{cat} and k_{cat}/K_M

	k_{cat} vs pH profile	k_{cat}/K_M vs pH profile
pH_{opt}	7.6	8.3
pK_{a1}	7.0 ± 0.1	7.7 ± 0.1
pK_{a2}	8.2 ± 0.1	8.9 ± 0.1

Table 2: Ligand Binding Properties of the NAD^+ and Mn^{2+} Cofactors

	K_d (μM) at pH 7.5	K_d (μM) at pH 8.4
NAD^+	17	29
Mn^{2+}	54	99

Determination of the K_d Value for NAD^+. GlvA was assayed in the presence of various concentrations of NAD^+, the enzyme being completely inactive in the absence of NAD^+. The data were fit to a simple hyperbolic binding equation and K_d values of 17 μM (pH 7.5) and 29 μM (pH 8.4) for the binding of dinucleotide cofactor to GlvA determined. The data are presented in Table 2.

Kinetic and Spectroscopic Investigation of Cofactor Reduction. The absorbance spectra (from 320 to 400 nm) of GlvA were recorded under three different conditions: 100 μM GlvA; 100 μM GlvA incubated with 100 μM NAD^+; and 100 μM GlvA incubated with 100 μM NAD^+ and 10 mM sodium borohydride (Figure 3). The peak in absorbance at 340 nm corresponding to NADH appears upon reduction with 10 mM sodium borohydride and is consistent with the quantitative reduction of NAD^+ to NADH. On the basis of the small K_d value of 17 μM (pH 7.5) for NAD^+, over 90% of GlvA has NAD^+ or NADH bound to its active site under these conditions, and very little remains free in solution. GlvA activity was assayed in the presence of NAD^+, and the activity was compared to that obtained in the presence

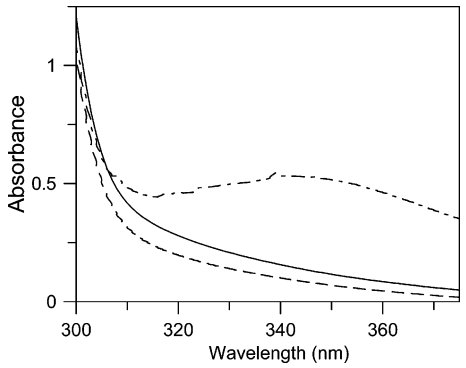

FIGURE 3: Absorbance spectra of GlvA with the dinucleotide cofactor in its oxidized (NAD^+) and reduced (NADH) states: 100 μM GlvA (apo) (—); 100 μM GlvA incubated with 100 μM NAD^+ (---); and 100 μM GlvA incubated with 100 μM NAD^+ and 10 mM sodium borohydride (EnDash− -).

of NADH (quantitatively reduced from NAD^+ using sodium borohydride) as shown in Figure 4. The enzyme was completely inactive in the presence of NADH (reduced form) alone. However, upon addition of excess NAD^+, full activity was rapidly restored (Figure 4). The loss of activity upon reduction was therefore solely attributable to the dinucleotide cofactor being present in the non-functional redox state (NADH), as opposed to protein denaturation or significant changes in pH of the assay solution.

Linear Free Energy Relationship: Brønsted Analysis. To determine whether cleavage of the glycosidic bond is itself rate-limiting, a Brønsted analysis was performed using four different 6-phospho-α-D-glucosides (34DNPαG6P, 4NPαG6P, PαG6P, M6′P, and MeαG6P). The pK_a values of the leaving groups range from 5.36 to 15.5 (Tables 3 and 4). Values of k_{cat} and K_M were determined for each substrate at pH 7.5 and 8.4, and the data are presented in Tables 3 and 4, respectively. The logarithms of k_{cat} and k_{cat}/K_M were calculated, and each was plotted against the pK_a of the leaving group. The Brønsted plots obtained are illustrated in Figure 5. As shown in Figure 5a and c, the k_{cat} value is independent of leaving group ability at both pH 7.5 and 8.4. The log k_{cat}/K_M values, however, display a small dependence on leaving group ability at pH 7.5 ($\beta = -0.17$) and at pH 8.4 ($\beta = -0.19$) as shown in Figure 5b and d, respectively.

A similar study was carried out with the β-linked substrates. Thus, linear free energy plots were generated using the following aryl 6-phospho-β-D-glucosides: 24DNPβG6P, 25DNPβG6P, 34DNPβG6P, 4Cl2NPβG6P, 4NPβG6P, 2NPβG6P, 35DCPβG6P, 3NPβG6P, 4CNPβG6P, and PβG6P. The pK_a values of the leaving groups range from 3.96 to 9.99. Values of k_{cat} and K_M were determined for each substrate at pH 7.5 and 8.4, and are presented in Tables 5 and 6, respectively. Again, the logarithms of k_{cat} and k_{cat}/K_M were calculated, and each was plotted against the pK_a of the leaving group. The Brønsted plots for the aryl 6-phospho-β-D-glucosides are shown in Figure 6a−d. Neither k_{cat} nor k_{cat}/K_M is significantly dependent on the phenol leaving group ability for aryl 6-phospho-β-D-glucosides.

Deuterium Kinetic Isotope Effect Measurements. Deuterium kinetic isotope effects for 1[^{2}H]4NPαG6P, 2[^{2}H]-4NPαG6P, 3[^{2}H]4NPαG6P, MeαG6P, 1[^{2}H]4NPβG6P, 2[^{2}H]-4NPβG6P, and 3[^{2}H]4NPβG6P were measured at two different substrate concentrations to give isotope effects on k_{cat} and on k_{cat}/K_M. All KIE data are summarized in Table 7.

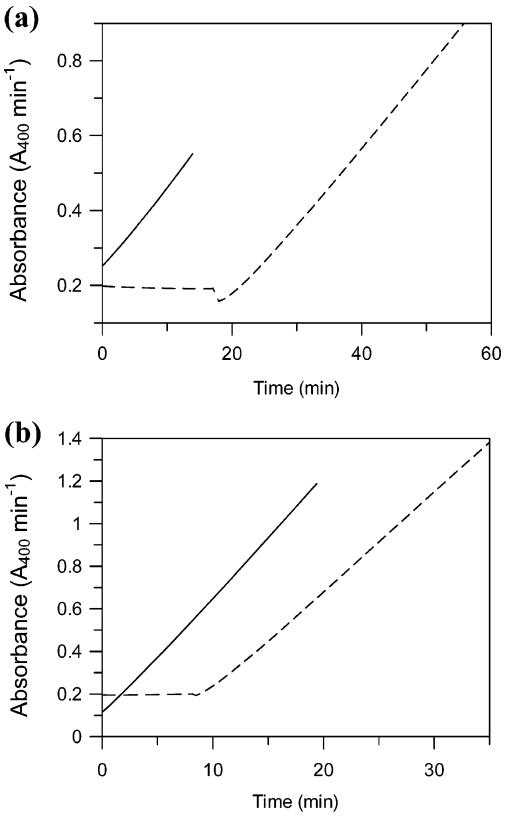

FIGURE 4: Assay of GlvA in the oxidized (NAD^+) and reduced (NADH) states. Observed rates of hydrolysis of 4NPαG6P by GlvA via the detection of 4-nitrophenolate release at 400 nm. In each case, the assay volume was 200 μL, and the concentration of GlvA used was 3.3 μg/mL. (a) pH 7.5, control (—): standard GlvA assay conditions, 50 mM HEPES (pH 7.5), 1 mM Mn^{2+}, 0.1 mM NAD^+, 10 mM 2-mercaptoethanol, and 0.1% (w/v) BSA at 37 °C. GlvA assay conditions (---): GlvA preincubated in 50 mM HEPES (pH 7.5), 1 mM Mn^{2+}, 0.1 mM NAD^+, 10 mM $NaBH_4$, 10 mM 2-mercaptoethanol, and 0.1% (w/v) BSA at 37 °C. No release of 4-nitrophenolate is observed until time = 18 min, when 2 nmol of NAD^+ was added. The activity was rapidly restored, and the catalytic rate is essentially the same as that of the sample without added $NaBH_4$; (b) pH 8.4, control (—): standard GlvA assay conditions, 50 mM Tris (pH 8.4), 1 mM Mn^{2+}, 0.1 mM NAD^+, 10 mM 2-mercaptoethanol, and 0.1% (w/v) BSA at 37 °C. GlvA assay conditions (---): GlvA preincubated in 50 mM Tris (pH 8.4), 1 mM Mn^{2+}, 0.1 mM NAD^+, 10 mM $NaBH_4$, 10 mM 2-mercaptoethanol, and 0.1% (w/v) BSA at 37 °C. No release of 4-nitrophenolate is observed until time = 8 min, when 2 nmol of NAD^+ was added. Activity was rapidly restored, and the catalytic rate is essentially the same as that of the sample without added $NaBH_4$.

Table 3: Michaelis−Menten Kinetic Parameters for the Hydrolysis of a Series of Aryl 6-Phospho-α-D-glucosides by GlvA at 37 °C in HEPES Buffer (pH 7.5)

6-phospho-α-D-glucoside	leaving group pK_a	k_{cat} (s^{-1})	K_M (μM)	k_{cat}/K_M (s^{-1}/mM)	$\Delta\epsilon$ ($M^{-1}cm^{-1}$)	λ_{max} (nm)
34DNPαG6P	5.36	0.72	12	61	14951	400
4NPαG6P	7.18	0.70	52	14	12618	400
PαG6P	9.99	0.90	69	13	1044	270
M6′P	13.00	1.3	4.0×10^2	3.3		
MeαG6P	15.5	0.42	6.1×10^2	0.69		

At pH 7.5, primary KIEs were measured for 3[^{2}H]4NPαG6P, 2[^{2}H]4NPβG6P, and 3[^{2}H]4NPβG6P. At pH 7.5, a unitary, or possibly a small inverse, KIE was determined for MeαG6P. No KIE was detected for 1[^{2}H]4NPαG6P or for 1[^{2}H]4NPβG6P. The KIE measured for 2[^{2}H]4NPαG6P at

Table 4: Michaelis−Menten Kinetic Parameters for the Hydrolysis of a Series of Aryl 6-Phospho-α-D-glucosides by GlvA at 37 °C in Tris-HCl Buffer (pH 8.4)

6-phospho-α-D-glucoside	leaving group pK_a	k_{cat} (s^{-1})	K_M (μM)	k_{cat}/K_M (s^{-1}/mM)	$\Delta\epsilon$ ($M^{-1}cm^{-1}$)	λ_{max} (nm)
34DNPαG6P	5.36	0.81	4.0	2.0×10^2	14720	400
4NPαG6P	7.18	0.85	14	60	17308	400
PαG6P	9.99	0.26	38	6.9	488	270
M6′P	13.00	1.3	3.6×10^2	3.6		
MeαG6P	15.5	1.1	5.0×10^2	2.2		

this pH falls in the range of either a small 1° KIE or a large 2° KIE. At pH 8.4, primary KIEs were measured for 3[^{2}H]-4NPαG6P, 2[^{2}H]4NPβG6P, and 3[^{2}H]4NPβG6P. Small inverse KIEs were measured for 1[^{2}H]4NPαG6P, 1[^{2}H]-4NPβG6P, and MeαG6P. Similar to what was determined at pH 7.5, the KIEs determined for 2[^{2}H]4NPαG6P also fall within the range of either a small 1° KIE or a large 2° KIE.

Inhibition of GlvA. Neither C6′P nor MeβG6P was hydrolyzed by GlvA. Both compounds were found to be competitive inhibitors of GlvA, with K_i values of 30 and 75 μM, respectively.

DISCUSSION

pH Dependence of GlvA Activity. The pH dependences of k_{cat}/K_M and k_{cat} (Figure 2a and b, respectively) both fit to classic bell-shaped curves but with slightly different pH optima of 8.4 and 7.6, respectively. Because two different pH_{opt} were obtained, all subsequent kinetic analyses were performed at both pH 7.5 (HEPES) and 8.4 (Tris). The two apparent pK_a values in the k_{cat}/K_M profile presumably represent ionizations of groups within the active site of the free enzyme or the free substrate that are critical to catalytic activity. The values obtained are reasonably close to those reported for BglT (7.08 ± 0.07 and 9.31 ± 0.08) (*15*), and as was proposed for BglT (*13*, *15*), the pK_a value of 7.68 ± 0.09 may correspond to that of the active site Tyr residue responsible for C2 deprotonation, which corresponds to Tyr265 in GlvA. Such a lowering of the pK_a value from its normal value of 10 for Tyr could easily be caused by its active site environment. Alternatively, this pK_a value could correspond to that of the phosphoryl moiety of the substrate if it binds only in the dianionic form. The origin of the pK_a value of 8.9 ± 0.1 is not at all clear, but it may represent the ionization of the conserved Arg residue that by X-ray crystallographic analysis is found to be within hydrogen-bonding distance of the phosphate group of the substrate (*16*). The dependence of k_{cat} upon pH reflects ionizations in the enzyme−substrate complex; thus, the small (0.7) pK_a differences observed relative to those determined from plots of k_{cat}/K_M vs pH are due to pK_a shifts upon complex formation.

Cofactor Specificity. It was previously shown that GlvA retained approximately 60% activity in the presence of the nicotinamide cofactor in its reduced form (NADH) (*10*). This report raised some concerns with respect to the proposed mechanism because NADH would be unable to carry out the initial oxidation of the C3 hydroxyl and thus render the enzyme inactive. However, the residual activity could have been an artifact due to a small amount of contaminating NAD^+ because NADH is readily oxidized to NAD^+ in aqueous solution. To address this issue, GlvA was dialyzed to remove any bound NAD^+, and the enzyme sample was found to be completely inactive. Full activity was restored in a saturable fashion by titration with NAD^+, yielding K_d values of 17 μM (pH 7.5) and 29 μM (pH 8.5). In separate experiments, inclusion of sodium borohydride in the assay also resulted in complete inactivation of GlvA, and UV−vis spectrophotometric analysis revealed that the NAD^+ cofactor had been reduced to NADH. Importantly, upon the addition of excess NAD^+, full activity was restored to the borohydride-treated sample, confirming that loss of activity was not due to enzyme denaturation. Clearly, NADH cannot activate GlvA, and this finding is consistent with the presently proposed mechanism.

Substrate Anomeric Specificity. Although maltose 6′-phosphate is the natural substrate for GlvA, surprisingly, GlvA also hydrolyzed 4NPβG6P, with kinetic parameters similar to those determined for the hydrolysis of 4NPαG6P (Tables 3−6). However, no hydrolysis of cellobiose 6′-phosphate or MeβG6P was observed, indicating that GlvA is only to able hydrolyze 6-phospho-β-glucosides containing highly activated leaving groups. GlvA is not unique in this regard because MalH from *Fusobacterium mortiferum*, another 6-phospho-α-glucosidase from GH4, has also been shown to hydrolyze substrates with activated leaving groups in both the α- and β-anomeric configurations (*27*). Reassuringly, analysis of the X-ray crystallographic data revealed that the +1 subsite of GlvA is large enough to accommodate substrates of both the α- and β-anomeric configurations (*15*). Kinetic characterization of GlvA was therefore performed using both aryl 6-phospho-α-glucosides and aryl 6-phospho-β-glucosides to determine whether GlvA utilizes the same mechanism for the hydrolysis of α- and β-glycosidic linkages and to gain more insight into details of that mechanism.

GlvA was previously shown to catalyze the hydrolysis of 4NPαG6P with a net retention of the anomeric configuration, yielding MeαG6P in the methanolysis reaction (*16*). However, in the current study, it was found that the enzyme catalyzes the hydrolysis of 4NPβG6P with net inversion of stereochemical configuration at C1, producing MeαG6P. Although this result would be bizarre for a glycosidase operating via a classical Koshland mechanism, the observation is consistent with the proposed mechanism. The elimination of the 4-nitrophenol leaving group from either 4NPαG6P or 4NPβG6P may not require acid catalysis and may proceed to form the same enediolate intermediate regardless of the substrate anomeric configuration. However, the 1,4-Michael-like addition to the α,β-unsaturated intermediate (common to both the hydrolysis of 4NPαG6P and 4NPβG6P) requires a properly positioned water molecule and most likely a general base catalyst to activate the water molecule for nucleophilic attack. Therefore, the anomeric configuration of the methanolysis product is independent of substrate anomeric configuration, in contrast to what is found with classical glycosidases. However, because GlvA hydrolyzes 6-phospho-α-glucopyranosides without activated leaving groups (such as M6′P) but not cellobiose 6′-phosphate (C6′P) or methyl 6-phospho-β-D-glucopyranoside (MeβGP) (data not shown), GlvA is certainly more appropriately classified as a 6-phospho-α-glucosidase than as a 6-phospho-β-glucosidase. The ability to hydrolyze β-glycosidic linkages

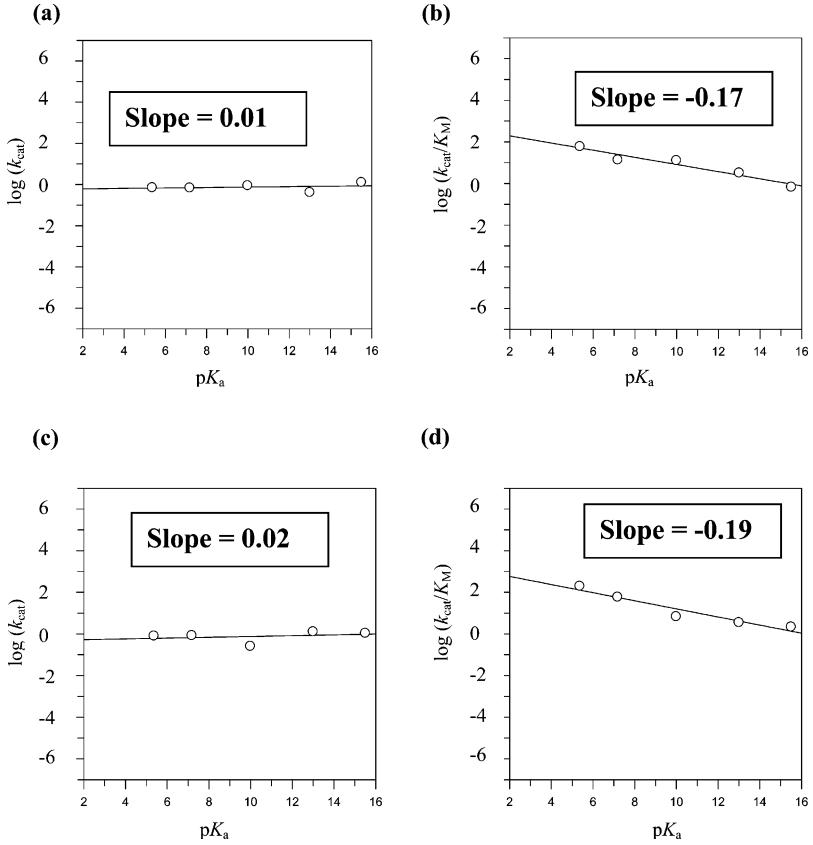

FIGURE 5: Brønsted plots for the enzymatic cleavage of various 6-phospho-α-D-glucosides: (a) log k_{cat} vs pK_a at pH 7.5; (b) log k_{cat}/K_M vs pK_a at pH 7.5; (c) log k_{cat} vs pK_a at pH 8.4; and (d) log k_{cat}/K_M vs pK_a at pH 8.4.

Table 5: Michaelis−Menten Kinetic Parameters for the Hydrolysis of a Series of Aryl 6-Phospho-β-D-glucosides by GlvA at 37 °C in HEPES Buffer (pH 7.5)

aryl 6-phospho-β-D-glucoside	phenol pK_a	k_{cat} (s^{-1})	K_M (μM)	k_{cat}/K_M (s^{-1}/mM)	$\Delta\epsilon$ ($M^{-1}cm^{-1}$)	λ_{max} (nm)
24DNPβG6P	3.96	0.27	35	7.5	9871	400
25DNPβG6P	5.15	0.25	1.3×10^2	2.0	4821	443
34DNPβG6P	5.36	0.42	2.9	1.5×10^2	14951	400
4Cl2NPβG6P	6.45	0.18	67	2.7	4498	428
4NPβG6P	7.18	0.52	54	9.6	12618	400
2NPβG6P	7.22	0.29	2.9×10^2	1.0	2155	413
35DCβG6P	8.19	0.66	27	24	1930	285
3NPβG6P	8.39	0.54	34	16	849	380
4CNPβG6P	8.49	0.64	1.2×10^2	5.5	6758	272
PβG6P	9.99	0.27	1.1×10^2	2.5	1044	270

Table 6: Michaelis−Menten Kinetic Parameters for the Hydrolysis of a Series of Aryl 6-Phospho-β-D-glucosides by GlvA at 37 °C in Tris-HCl Buffer (pH 8.4)

aryl 6-phospho-β-D-glucoside	phenol pK_a	k_{cat} (s^{-1})	K_M (μM)	k_{cat}/K_M (s^{-1}/mM)	$\Delta\epsilon$ ($M^{-1}cm^{-1}$)	λ_{max} (nm)
24DNPβG6P	3.96	0.63	41	16	9903	400
25DNPβG6P	5.15	0.46	73	6.3	4035	443
34DNPβG6P	5.36	0.36	1.9	1.9×10^2	14720	400
4Cl2NPβG6P	6.45	0.52	75	6.8	4152	428
4NPβG6P	7.18	0.34	24	14	17308	400
2NPβG6P	7.22	0.40	3.0×10^2	1.3	4581	413
35DCβG6P	8.19	0.47	3.8	1.2×10^2	2387	285
3NPβG6P	8.39	0.97	8.9	1.1×10^2	1289	380
4CNPβG6P	8.49	0.32	28	11	14008	272
PβG6P	9.99	1.1	23	52	488	270

is exceptional and applies only to activated 6-phospho-β-D-glucopyranosides.

Mechanistic Investigation via KIE and Brønsted Analysis. Careful analysis of the rather large body of kinetic data on the GlvA-catalyzed hydrolysis of both the α- and β-glycosides provides insights not only into the general mechanism followed but also into some clue as to the general shape of the reaction coordinate diagram. Although the KIEs and Brønsted analyses of the 6-phospho-β-glucosides are in agreement with those observed for 6-phospho-α-glucosides, some caution regarding the interpretation of the data for the 6-phospho-β-glucosides is merited, particularly in light of the fact that GlvA is unable to hydrolyze the glycosidic linkage of naturally occurring phospho-β-glucosides. The first general conclusion is that the overall mechanism proposed in Figure 1 is fully supported by the kinetic data. First, the measurement of primary KIEs on both k_{cat} and k_{cat}/K_M, and for both the 3[^{2}H]4NPαG6P and 3[^{2}H]4NPβG6P, at both pH values, is completely consistent with the proposed oxidation at C3 and with this step being at least partially rate-limiting for both classes of substrate. Indeed, it is difficult to envisage any other mechanism that would give rise to such an isotope effect at C3. This finding is also consistent with the fact that, even in the presence of substrate, the enzyme exists primarily in its NAD^+ form, as observed spectrophotometrically. Second, the measurement of isotope effects that are clearly primary for the 2[^{2}H]4NPβG6P is fully consistent with a deprotonation event at C2 that is at least partially rate-limiting. Those measured at C2 for 2[^{2}H]4NPαG6P are considerably smaller but still consistent with such a mechanism. Third, the absence of any dependence of k_{cat} on leaving group ability is consistent with relatively rapid and non-rate-limiting glycosidic bond cleavage. This is fully supported by the absence of normal secondary deuterium

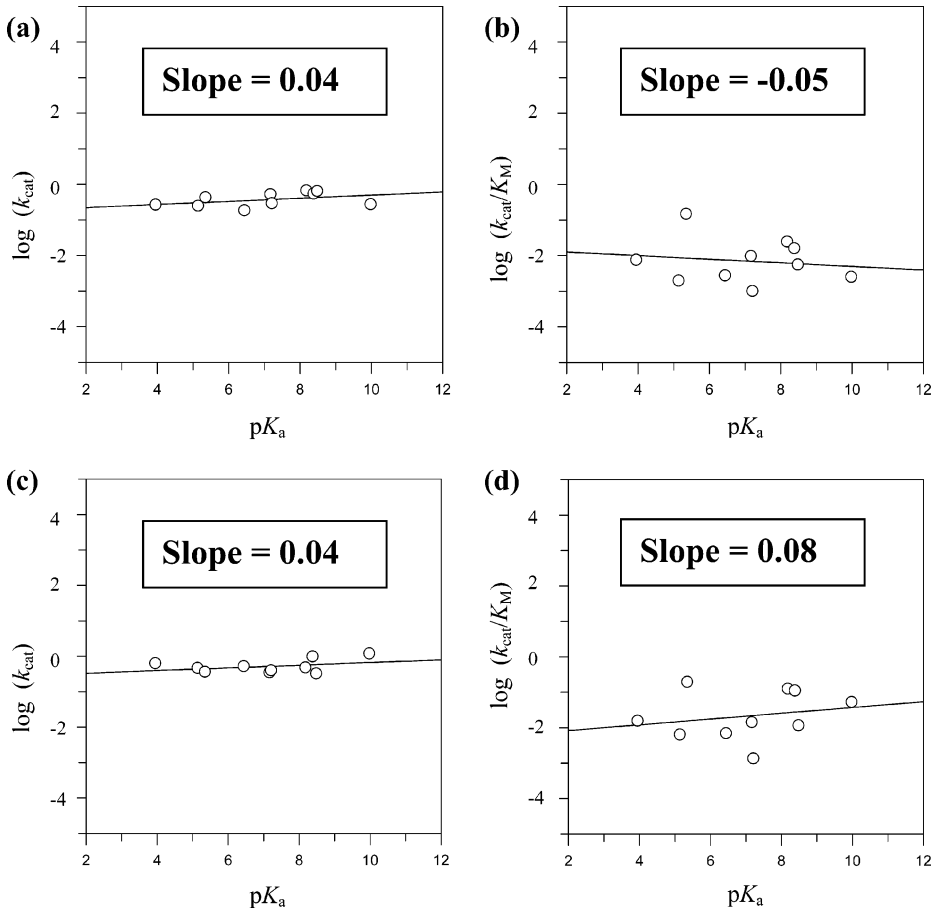

FIGURE 6: Brønsted plots for the enzymatic cleavage of various aryl 6-phospho-β-D-glucosides: (a) log k_{cat} vs pK_a at pH 7.5; (b) log k_{cat}/K_M vs pK_a at pH 7.5; (c) log k_{cat} vs pK_a at pH 8.4; and (d) log k_{cat}/K_M vs pK_a at pH 8.4.

Table 7: Kinetic Isotope Effect Measurements for Deuterated Substrates of GlvA

	$(k_{cat})H/(k_{cat})_D$ (pH 7.5)	$(k_{cat}/K_M)_H/(k_{cat}/K_M)_D$ (pH 7.5)	$(k_{cat})_H/(k_{cat})_D$ (pH 8.4)	$(k_{cat}/K_M)_H/(k_{cat}/K_M)_D$ (pH 8.4)
1[^{2}H]4NPαG6P	0.99 ± 0.02	1.01 ± 0.04	0.88 ± 0.01	1.0 ± 0.1
2[^{2}H]4NPαG6P	1.21 ± 0.02	1.28 ± 0.07	1.14 ± 0.01	1.30 ± 0.09
3[^{2}H]4NPαG6P	1.73 ± 0.02	1.59 ± 0.05	1.82 ± 0.02	2.2 ± 0.3
1[^{2}H]MeαG6P	0.96 ± 0.02	0.98 ± 0.04	0.93 ± 0.01	0.94 ± 0.03
1[^{2}H]4NPβG6P	1.00 ± 0.01	1.00 ± 0.06	0.89 ± 0.01	0.99 ± 0.03
2[^{2}H]4NPβG6P	3.52 ± 0.02	6.4 ± 0.5	1.76 ± 0.02	3.2 ± 0.2
3[^{2}H]4NPβG6P	1.70 ± 0.02	1.89 ± 0.09	1.89 ± 0.02	2.2 ± 0.1

KIEs for the 1-[^{2}H]-6-phospho-glucoside substrates. Overall, these data strongly support a redox-activated $E1_{cb}$ mechanism for this enzyme.

A closer look at the data and particularly a comparison of k_{cat} and k_{cat}/K_M data for the 6-phospho-α- and 6-phospho-β-glucosides provides further insights, particularly into the general shape of the reaction coordinate diagrams for the two substrates. It is worth noting that the most useful sets of kinetic isotope effects to evaluate are those determined at the pH optimum for that parameter. This would mean the KIEs on k_{cat} determined at pH 7.5 and the KIEs on k_{cat}/K_M measured at pH 8.4. Indeed, the pairs of values measured in these cases are quite similar, suggesting that the two kinetic parameters may well be reflecting the same chemical step at their respective pH_{opt}.

GlvA catalyzes the hydrolysis of 4NPαG6P and 4NPβG6P with similar k_{cat} values, which is consistent with the conclusion arrived at above that steps that do not critically depend on the substrate anomeric configuration are rate-limiting for these two classes of substrate, namely, oxidation at C3 and deprotonation at C2. A key *difference* in the data for the two substrates is in the values of the KIEs for 2[^{2}H]-4NPαG6P and 2[^{2}H]4NPβG6P. Very large KIEs are seen for the β-glycoside, particularly, at the lower pH, suggesting that this deprotonation step is more fully rate-limiting than is the case for the α-glycoside substrates. (Though surprisingly for this interpretation, the KIE measured for 3[^{2}H]-4NPβG6P is not correspondingly lowered.) Interestingly, at the higher pH value, the KIE for the 2[^{2}H]4NPβG6P is lower than that measured at the lower pH value. This is as expected because proton abstraction should be faster in the presence of a higher concentration of the conjugate base under more basic conditions. Values of KIEs for 2[^{2}H]4NPαG6P are much lower; indeed on the borderline with values of large secondary deuterium KIEs that would be associated with a rate-limiting breakage of the glycosidic bond. However, this latter scenario cannot be the case, at least for k_{cat}, because no dependence of k_{cat} upon aglycone pK_a was observed

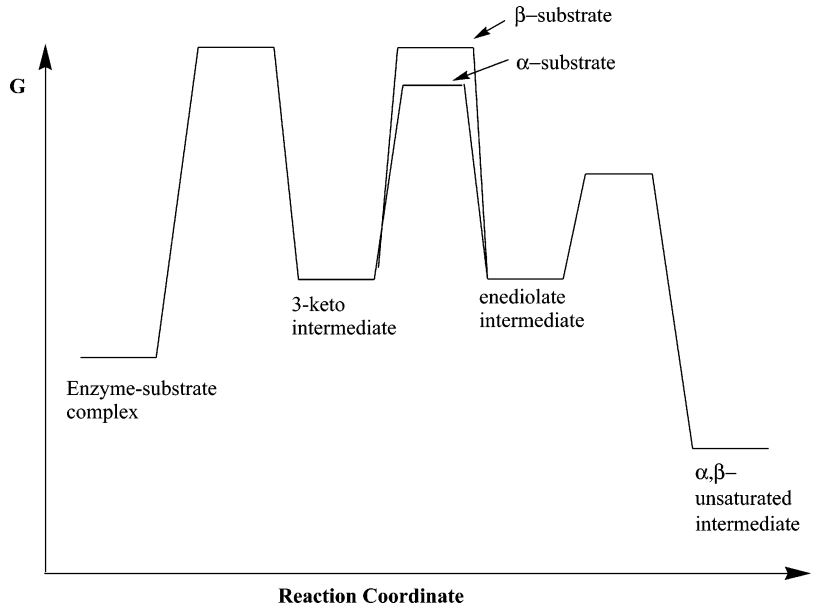

FIGURE 7: Graphical representation of the reaction coordinate for the GlvA-catalyzed hydrolysis of α- and *β*-substrates.

(Figure 5). It is therefore probable that these are small primary KIEs whose lower magnitude either reflects a smaller contribution of that step to the rate-limiting process or a highly asymmetric transition state for deprotonation, which results from either an early or, more probably, a late transition state. Given its natural substrate specificity, GlvA presumably evolved to cleave α-glycosides, for which its acid and base catalysts are optimally positioned. When operating on *β*-glycosides, the acid catalyst assisting C1−O1 cleavage is certainly out of position, hence the lack of action on unactivated substrates of this anomeric stereochemistry, such as the Me*β*G6P and C6′P. It is also likely that the accommodation of the aryl aglycone of the *β*-glucosides within the active site may result in some displacement of the base catalyst from its optimal position, making deprotonation less efficient, thus more fully rate-limiting. The tempting alternative explanation that the mechanism for cleavage of α-glycosides is more-E2 like given the transperiplanar arrangement of the C2−H2 bond and the glycosidic bond is rendered untenable by the absence of any leaving group dependence on k_{cat}.

Because C6′P and Me*β*G6P are not hydrolyzed by GlvA, the Brønsted plots generated from k_{cat} (Figure 6a and c) and k_{cat}/K_M for the hydrolysis of aryl *β*-glycosides (Figure 6b and d) were only available for leaving groups with pK_a values ranging from 3.96 to 9.99. Both log k_{cat} and log k_{cat}/K_M versus pK_a at both pH 7.5 and 8.4 produced flat linear free-energy relationships. Although the log k_{cat}/K_M versus pK_a plots displayed a high level of scattering, likely due to differential interactions of the variously substituted aryl rings with an active site that had not evolved a cavity at this location, there is clearly no significant systematic dependence upon leaving group ability. These flat linear free-energy relationships, in conjunction with the lack of a secondary KIE for 1[^{2}H]-4NP*β*G6P ($(k_{cat})_H/(k_{cat})_D$) show that cleavage of the C1−O1 linkage is not rate-limiting for aryl 6-phospho-*β*-glucoside substrates.

Likewise, the lack of dependence of k_{cat} for the hydrolysis of the aryl α-glucosides on aglycone pK_a at both pH 7.5 and 8.4 shows that glycoside bond cleavage is not rate-limiting in that case either (Figure 5a and c), though small dependences of k_{cat}/K_M upon leaving group ability are seen. Comparison and interpretation of data based upon k_{cat}/K_M require prior consideration of the meaning of that parameter in this case. Normally, k_{cat}/K_M is assumed to reflect the first irreversible step, which would appear to be cleavage of the glycosidic bond. However, if this step is fast compared to the prior proton-transfer step, as seems to be the case, the deprotonation step would also be rendered essentially irreversible. Likewise, if deprotonation is faster than the redox process, then k_{cat}/K_M may also reflect contributions from the oxidation step. This could explain why substantial KIEs are seen in k_{cat}/K_M for both 2[^{2}H]- and 3[^{2}H]-substrates, which otherwise would not be expected to exhibit primary KIEs if k_{cat}/K_M purely reflected the bond cleavage step. Indeed, as noted above, when the KIEs on k_{cat} at pH 7.5 and k_{cat}/K_M at pH 8.4 are compared, they are indeed very similar within each isotopomer pair, consistent with the same step being reflected. Such a situation demands a general reaction coordinate diagram such as that shown in Figure 7 for the first half of the reaction, up to the formation of the α,*β*-unsaturated intermediate. The assignment of energy levels in this diagram is arbitrary: their measurement would be non-trivial because it would require the determination of partition ratios for all of the species along the coordinate. However, the generalized diagram is a useful way of thinking about rate constants and how they differ for the two substrates. The barrier heights are shown as being similar across the coordinate, as required by the presence of isotope effects on H3, H2, and, even in one case, also on H1. However, the highest barrier for the α-glycoside substrates is that for the oxidation step, whereas the highest for the *β*-glycoside substrates is that for the proton abstraction, as dictated by the large primary KIE on the 2[^{2}H]-substrate.

The origin of the inverse secondary deuterium KIE measured at high pH for the 1[^{2}H]MeαG6P (on both k_{cat} and k_{cat}/K_M) and for 1[^{2}H]4NPαG6P on k_{cat} (nonoptimal pH) is unclear. Interestingly, the k_{cat} values measured in these three situations are among the highest of all the k_{cat} values measured. This suggested at the outset that a step subsequent

to C1−O1 bond cleavage in which an sp^2 hybridized anomeric center is being converted to an sp^3 center, for example, addition of water to the Michael acceptor intermediate, might be the rate-limiting step. However, methanol competition experiments (not shown) revealed no rate enhancements under conditions where methanol is known to act as a superior nucleophile, as was seen in the use of methanol as a superior acceptor in NMR-based stereochemical outcome determinations (*15*). Therefore, this step cannot be rate-limiting.

CONCLUSIONS

A detailed analysis of the proposed $E1_{cb}$ mechanism of GlvA is provided by the kinetic data presented. The first, partially rate-limiting step involves the essential NAD^+-mediated oxidation of the C3 hydroxyl to a ketone. As a result, the C2 proton is activated for deprotonation by the adjacent carbonyl and potentially by polarization of the enediolate intermediate by the metal cation found at the enzyme active site. Subsequent to the second, partially rate-limiting C2 proton abstraction, rapid elimination of the C1−O1 linkage occurs to generate an α,β-unsaturated Michael acceptor, which undergoes an addition reaction with a water molecule. Finally, reduction of the C3 ketone by the on-board NADH cofactor yields the overall hydrolysis product. The proposed $E1_{cb}$ mechanism of GlvA is evidently the same as that described for BglT. Importantly, the key catalytic residues for this mechanism are those that interact with the 2- and 3-positions of the substrate, rather than those that interact with the anomeric center or the glycosidic oxygen. Indeed, acid/base catalysis of aglycone departure and water attack will be of much less importance for this mechanism than for the standard oxocarbenium ion mechanism of normal glycosidases. This likely explains why Family 4 contains both α- and β-glycosidases and why some members such as GlvA can hydrolyze both α- and β-glycosides containing activated leaving groups.

Interestingly, a new glycosidase family (GH109) that also uses NAD^+ for catalysis has recently been reported (*28*). The location of the cofactor at the active site and the observation of deuterium incorporation at C2 when the reaction is performed in D_2O both suggest a similar reaction mechanism. It will be interesting to see how many other glycosidases use this unexpected means of glycosidic bond cleavage.

ACKNOWLEDGMENT

We thank our collaborators Dr. G. J. Davies and Dr. A. Varrot for structural analyses and express appreciation to Dr. Andreas Pikis for excellent technical assistance and constructive criticism.

REFERENCES

1. Henrissat, B., and Bairoch, A. (1996) Updating the sequence-based classification of glycosyl hydrolases, *Biochem. J. 316*, 695−696.
2. Henrissat, B., and Davies, G. (1997) Structural and sequence-based classification of glycoside hydrolases, *Curr. Opin. Struct. Biol. 7*, 637−644.
3. Henrissat, B., Callebaut, I., Fabrega, S., Lehn, P., Mornon, J. P., and Davies, G. (1995) Conserved catalytic machinery and the prediction of a common fold for several families of glycosyl hydrolases, *Proc. Natl. Acad. Sci. U.S.A. 92*, 7090−7094.
4. Koshland, D. E., Jr. (1953) Stereochemistry and the mechanism of enzymic reactions, *Biol. Rev. 28*, 416−436.
5. Zechel, D. L., and Withers, S. G. (2000) Glycosidase mechanisms: anatomy of a finely tuned catalyst, *Acc. Chem. Res. 33*, 11−18.
6. Sinnott, M. L. (1990) Catalytic mechanisms of enzymatic glycosyl transfer, *Chem. Rev. 90*, 1171−1202.
7. Bouma, C. L., Reizer, J., Reizer, A., Robrish, S. A., and Thompson, J. (1997) 6-Phospho-α-D-glucosidase from *Fusobacterium mortiferum*: cloning, expression, and assignment to family 4 of the glycosylhydrolases, *J. Bacteriol. 179*, 4129−4137.
8. Raasch, C., Armbrecht, M., Streit, W., Höcker, B., Sträter, N., and Liebl, W. (2002) Identification of residues important for NAD^+ binding by the *Thermotoga maritima* α-glucosidase AglA, a member of glycoside hydrolase family 4, *FEBS Lett. 517*, 267−271.
9. Thompson, J., Robrish, S. A., Immel, S., Lichtenthaler, F. W., Hall, B. G., and Pikis, A. (2001) Metabolism of sucrose and its five linkage-isomeric α-D-glucosyl-D-fructoses by *Klebsiella pneumoniae*: participation and properties of sucrose-6-phosphate hydrolase and phospho-α-glucosidase, *J. Biol. Chem. 276*, 37415−37425.
10. Thompson, J., Pikis, A., Ruvinov, S. B., Henrissat, B., Yamamoto, H., and Sekiguchi, J. (1998) The gene *glvA* of *Bacillus subtilis* 168 encodes a metal-requiring, NAD(H)-dependent 6-phospho-α-glucosidase: assignment to family 4 of the glycosylhydrolase superfamily, *J. Biol. Chem. 273*, 27347−27356.
11. Thompson, J., Gentry-Weeks, C. R., Nguyen, N. Y., Folk, J. E., and Robrish, S. A. (1995) Purification from *Fusobacterium mortiferum* ATCC 25557 of a 6-phosphoryl-*O*-α-D-glucopyranosyl:6-phosphoglucohydrolase that hydrolyzes maltose 6-phosphate and related phospho-α-D-glucosides, *J. Bacteriol. 177*, 2505−2512.
12. Thompson, J., Ruvinov, S. B., Freedberg, D. I., and Hall, B. G. (1999) Cellobiose-6-phosphate hydrolase (CelF) of *Escherichia coli*: characterization and assignment to the unusual family 4 of glycosylhydrolases, *J. Bacteriol. 181*, 7339−7345.
13. Yip, V. L. Y., Varrot, A., Davies, G. J., Rajan, S. S., Yang, X. J., Thompson, J., Anderson, W. F., and Withers, S. G. (2004) An unusual mechanism of glycoside hydrolysis involving redox and elimination steps by a family 4 β-glycosidase from *Thermotoga maritima*, *J. Am. Chem. Soc. 126*, 8354−8355.
14. Yip, V. L. Y., and Withers, S. G. (2006) Mechanistic analysis of the unusual redox-elimination sequence employed by *Thermotoga maritima* BglT: a 6-phospho-β-glucosidase from glycoside hydrolase family 4, *Biochemistry 45*, 571−580.
15. Varrot, A., Yip, V. L. Y., Li, Y., Rajan, S. S., Yang, X., Anderson, W. F., Thompson, J., Withers, S. G., and Davies, G. J. (2005) NAD^+ and metal-ion dependent hydrolysis by family 4 glycosidases: structural insight into specificity for phospho-β-D-glucosides, *J. Mol. Biol. 346*, 423−435.
16. Rajan, S. S., Yang, X., Collart, F., Yip, V. L. Y., Withers, S. G., Varrot, A., Thompson, J., Davies, G. J., and Anderson, W. F. (2004) Novel catalytic mechanism of glycoside hydrolysis based on the structure of an NAD^+/Mn^{2+}-dependent phospho-α-glucosidase from *Bacillus subtilis*, *Structure 12*, 1619−1629.
17. Sowa, W., and Thomas, G. H. S. (1966) Oxidation of 1,2-5,6-di-*O*-isopropylidene-D-glucose by dimethyl sulfoxide-acetic anhydride, *Can. J. Chem. 44*, 836−838.
18. Koch, H. J., and Perlin, A. S. (1970) Synthesis and ^{13}C N.M.R. spectrum of D-glucose-3-d. bond-polarization differences between the anomers of D-glucose, *Carbohydr. Res. 15*, 403−410.
19. Audichya, T. D., Ingle, T. R., and Bose, J. L. (1971) Studies in the stannic chloride catalysed glycosidation of phenols, *Indian J. Chem. 9*, 315−317.
20. Lee, S. S., Yu, S., and Withers, S. G. (2003) Detailed dissection of a new mechanism for glycoside cleavage: α-1,4-glucan lyase, *Biochemistry 42*, 13081−13090.
21. Ballardie, F., Capon, B., Sutherland, J. D. G., Cocker, D., and Sinnott, M. L. (1973) A simple general synthesis of 2,4-dinitrophenyl glycopyranosides, *J. Chem. Soc., Perkin Trans. 1*, 2418−2419.
22. Sinnott, M. L., and Souchard, I. J. L. (1973) Mechanism of action of β-galactosidase: effect of aglycone nature and α-deuterium substitution on hydrolysis of aryl galactosides, *Biochem. J. 133*, 89−98.
23. Wilson, G., and Fox, C. F. (1974) The β-glucoside system of *Escherichia coli*. IV. Purification and properties of phospho-β-glucosidases A and B, *J. Biol. Chem. 249*, 5586−5598.

24. Cawley, T. N., and Letters, R. (1971) Phosphate migration in some phosphate monoesters and diesters of methyl α-D-mannopyranoside, *Carbohydr. Res. 19*, 373−382.
25. Joshi, M. D., Sidhu, G., Pot, I., Brayer, G. D., Withers, S. G., and McIntosh, L. P. (2000) Hydrogen bonding and catalysis: a novel explanation for how a single amino acid substitution can change the pH optimum of a glycosidase, *J. Mol. Biol. 299*, 255−279.
26. Kempton, J. B., and Withers, S. G. (1992) Mechanism of *Agrobacterium β*-glucosidase: kinetic studies, *Biochemistry 31*, 9961−9969.
27. Pikis, A., Immel, S., Robrish, S. A., and Thompson, J. (2002) Metabolism of sucrose and its five isomers by *Fusobacterium mortiferum*, *Microbiology 148*, 843−852.
28. Liu, Q. P., Sulzenbacher, G., Yuan, H., Bennett, E. P., Pietz, G., Saunders, K., Spence, J., Nudelman, E., Levery, S. B., White, T., Neveu, J. M., Lane, W. S., Bourne, Y., Olsson, M. L., Henrissat, B., and Clausen, H. (2007) Bacterial glycosidases for the production of universal red blood cells, *Nat. Biotechnol. 25*, 454−464.

BI700536P